Uneven Grid-based Linear Parameter-Varying Controller Design for Guided Projectiles

Gian Marco Vinco, Spilios Theodoulis, Olivier Sename, Guillaume Strub

Uneven Grid-based Linear Parameter-Varying Controller Design for Guided Projectiles

G.M. Vinco [*,**] **S. Theodoulis** [***] **O. Sename** [**] **G. Strub** [*]

[*] *French-German Research Institute of Saint-Louis, 68300, Saint-Louis, France (e-mail: guillaume.strub@isl.eu).*
[**] *University Grenoble Alpes, CNRS, Grenoble INP, GIPSA-Lab, 38000, Grenoble, France (e-mail: gian-marco.vinco@grenoble-inp.fr, olivier.sename@grenoble-inp.fr).*
[***] *Delft University of Technology, Faculty of Aerospace Engineering, 2629, Delft, The Netherlands (e-mail: S.Theodoulis@tudelft.nl)*[1].

Abstract: This paper proposes a Linear Parameter-Varying (LPV) controller design for the pitch channel dynamics of a new class of Long Range Guided Projectiles (LRGP). The grid-based approach is preferred since it provides advantages in terms of performance and conservatism. Differently from standard aerospace applications that limit the scheduling vector to the variation of the altitude and the Mach number, the investigated flight envelope is parameterized through a 3D grid, which includes the variation of the angle-of-attack, crucial for range optimization purposes. Thus, an extensive investigation of the grid design is required to minimize the computational complexity of the controller synthesis. The performances of the LPV controller are assessed by employing a nonlinear reference tracking simulation scenario.

Keywords: Guidance, navigation and control of vehicles, Linear parameter-varying systems, Time-varying systems

1. INTRODUCTION

The gain-scheduling design is a standard approach in the framework of aerospace flight control. The investigated flight envelope is parameterized as a grid of selected parameters (usually altitude and Mach), varying in a specified range. The nonlinear models are linearized at each grid point, obtaining a set of local Linear Time-Invariant (LTI) realizations of the system, which forms the generalized Linear Parameter-Varying (LPV) model. The controller at any conditions of the flight envelope is synthesized through the interpolation of the corresponding set of local LTI controllers, designed at each grid point (Theodoulis et al. (2015); Gruenwald and Bryson (2022)).

However, the linearized models provide only locally reliable representations of the nonlinear systems. Additionally, no a priori guarantees about the stability and the performance of the local controllers' interpolation are provided at generic flight points and for arbitrary variation rates of the scheduling parameters (Shamma and Athans (1992); Biannic and Apkarian (1999)). A widespread design solution consists of extending the linearization on a dense grid of conditions, and a posteriori, testing the controller robustness on a much denser grid. Nevertheless, this process requires time and high computational power since it generates a large number of local LTI controllers to be implemented and used in the interpolation.

In this context, we propose a grid-based LPV control design applied to a new class of *Long Range Guided Projectiles* (LRGP). The LPV projectile's model was obtained through the State Transformation technique discussed in (Vinco et al. (2022b)). The controller synthesis grid-based design relies on the resolution of a set of Linear Matrix Inequalities (LMIs), employing parameter-dependent Lyapunov functions and accounting for both parameters' variation range and rate of variation (Bryson and Gruenwald (2022); Sato (2022)). A common parameterization is established for the controller's synthesis at each grid point, favoring the possibility that the stability and performance properties guaranteed at the grid points are also met at intermediate flight conditions through interpolation. The flight envelope is parameterized in an *uneven* fashion, based on an ad-hoc designed range-extending guidance law, to optimize the controller synthesis performances.

The projectile's nonlinear dynamics and the corresponding grid-based LPV model are first presented in Section 2. Section 3 discusses the general formulation of grid-based LPV controller synthesis, providing an overview of the controller design architecture. In Section 4, an analysis of each of the investigated scheduling parameters suggests the size of the grid parameterization, later employed in the controller synthesis. Finally, in Section 5 the controller performances are tested both in the frequency domain and on a guidance trajectory tracking simulation.

[1] The author was with the French-German Research Institute of Saint-Louis, 68300, Saint-Louis, France. He is now with Delft University of Technology, Control & Operations Department, Faculty of Aerospace Engineering, 2629, Delft, The Netherlands.

2. PROJECTILE MODEL FORMULATION

In this paper, we focus the control design on the pitch channel dynamics of a 155 mm fin-stabilized guided projectile. The concept is characterized by two front canards which allow for induced pitching and rolling moment control actions along the longitudinal and lateral axes. The authority is achieved, respectively, by means of a concurrent or a differential combination of the individual canards' local deflection. A set of four symmetrical rear fins is mounted in a non co-planar fashion with the canards' plane to reduce the aerodynamic interaction and improve stability. In the following, only the main features concerning the nonlinear and the LPV model description are recalled. Exhaustive explanations are provided in Vinco et al. (2022a) and Vinco et al. (2022b), respectively.

2.1 Projectile Pitch Dynamics Model

By reason of the planar symmetrical structure of the projectile, and assuming an operating gliding trajectory characterized by a Bank-to-Turn (BTT) flight strategy, the pitch and the lateral channel dynamics of the projectile are decoupled in the analysis. Consequently, the lateral influence of the angle-of-sideslip, β, and the yaw rate r, as well as the roll angle, ϕ, and the roll rate, p, are assumed negligible. Additionally, $\bar{\theta}$ represents a baseline value for the pitch angle. The resulting nonlinear pitch channel dynamics can be expressed through the following angle-of-attack, α, and pitch rate, q, dynamics:

$$\begin{aligned}\dot{\alpha} =& -\frac{F_X \sin\alpha}{mV} + \frac{F_Z \cos\alpha}{mV} \\ &+ \frac{g}{V}(\sin\alpha\sin\bar{\theta} + \cos\alpha\cos\bar{\theta}) + q, \\ \dot{q} =& \frac{M}{I_{yy}},\end{aligned} \tag{1}$$

including the projectile mass, m, the acceleration of gravity, g, and the moment of inertia related to the y-axis, I_{yy}. The air mass is assumed at rest, implying no relative wind affecting the airspeed, V. The aerodynamic longitudinal force, F_X, vertical force, F_Z, and pitching moment, M have been modeled by means of an extensive regression analysis on a dataset of Computational Fluid Dynamics (CFD) simulations, as follows:

$$\begin{aligned}F_X &= \bar{q}SC_{X_\mathrm{S}}(\mathcal{M},\alpha), \\ F_Z &= \bar{q}S\left[C_{Z_\mathrm{S}}(\mathcal{M},\alpha) + \left(\frac{d}{2V}\right)C_{Z_q}(\mathcal{M})q + C_{Z_{\delta_q}}(\mathcal{M})\delta_q\right], \\ M &= \bar{q}Sd\left[C_{m_\mathrm{S}}(\mathcal{M},\alpha) + \left(\frac{d}{2V}\right)C_{m_q}(\mathcal{M})q + C_{m_{\delta_q}}(\mathcal{M})\delta_q\right].\end{aligned} \tag{2}$$

The reference caliber, d, defines the reference surface, $S = \frac{\pi d^2}{4}$, while the altitude, h, affects the air density value, and consequently, the dynamic pressure, $\bar{q}$. The set of static aerodynamic coefficients, C_{X_S}, C_{Z_S}, and C_{m_S}, is expressed as a function of the Mach number, $\mathcal{M}$, and was obtained as a result of the regression analysis. Similarly, C_{Z_q} and C_{m_q} correspond to the vertical and pitching damping coefficients, while $C_{Z_{\delta_q}}$ and $C_{m_{\delta_q}}$, are the control ones. The extended expressions of the aerodynamic model for the pitch channel dynamics are described in Vinco et al. (2022a). Finally, δ_q stands for the combined concurrent local pitch deflection of the right and left canards, representing the only control input of the system. The angle-of-attack and the pitch rate are supposed to be available measurements, as well as the normal acceleration:

$$\eta_z = \frac{\bar{q}S}{mg}\left[C_{Z_\mathrm{S}}(\mathcal{M},\alpha) + \left(\frac{d}{2V}\right)C_{Z_q}(\mathcal{M})q + C_{Z_{\delta_q}}(\mathcal{M})\delta_q\right].$$

2.2 Grid-based quasi-LPV Model

The interested reader may find the extended modeling process in Vinco et al. (2022b). The quasi-LPV model of the pitch channel dynamics has been obtained through the *State Transformation* of Eqs. (1)-(2), introduced in Shamma (1988). This approach aims to hide the nonlinearities present in the model, by the definition of the off-equilibrium non-scheduling state, $q_\mathrm{dev} = q - q_\mathrm{eq}$, and control input, $\delta_{q,\mathrm{dev}} = \delta_q - \delta_{q,\mathrm{eq}}$. The transformation is achieved through a set of equilibrium functions, q_eq and $\delta_{q,\mathrm{eq}}$, evaluated by trimming Eqs. (1)-(2) across the flight envelope. Additionally, the system is augmented with an integrator at the input, $\sigma = \int \delta_q$. The scheduling vector accounts for the angle-of-attack variation as an endogenous parameter, to complete the standard exogenous ones: airspeed and altitude, $\rho(t) = [\alpha(t),\ V(t),\ h(t)]$. The off-equilibrium acceleration measurements are also defined as $\eta_{z,\mathrm{dev}} = \eta_z(q,\delta_q) - \eta_z(q_\mathrm{eq},\delta_{q,\mathrm{eq}})$. The quasi-LPV model is then expressed as:

$$\begin{bmatrix}\dot{\alpha}\\ \dot{q}_\mathrm{dev}\\ \dot{\delta}_{q,\mathrm{dev}}\end{bmatrix} = \begin{bmatrix}0 & A_{12}(\rho) & B_1(\rho)\\ 0 & \tilde{A}_{22}(\rho) & \tilde{B}_2(\rho)\\ 0 & \tilde{A}_{32}(\rho) & \tilde{B}_3(\rho)\end{bmatrix}\begin{bmatrix}\alpha\\ q_\mathrm{dev}\\ \delta_{q,\mathrm{dev}}\end{bmatrix} + \begin{bmatrix}0\\0\\I\end{bmatrix}\sigma, \tag{3}$$

$$\begin{bmatrix}\alpha\\ q_\mathrm{dev}\\ \eta_{z,\mathrm{dev}}\end{bmatrix} = \begin{bmatrix}1 & 0 & 0\\ 0 & 1 & 0\\ 0 & \tilde{C}_{32}(\rho) & \tilde{C}_{33}(\rho)\end{bmatrix}\begin{bmatrix}\alpha\\ q_\mathrm{dev}\\ \delta_{q,\mathrm{dev}}\end{bmatrix}, \tag{4}$$

where:

$$\begin{aligned}&\tilde{A}_{22}(\rho) \coloneqq A_{22}(\rho) - \frac{\partial q_\mathrm{eq}}{\partial\alpha}A_{12}(\rho);\ \tilde{A}_{32}(\rho) \coloneqq -\frac{\partial\delta_{q,\mathrm{eq}}}{\partial\alpha}A_{12}(\rho),\\ &\tilde{B}_2(\rho) \coloneqq B_2(\rho) - \frac{\partial q_\mathrm{eq}}{\partial\alpha}B_1(\rho); \quad \tilde{B}_3(\rho) \coloneqq -\frac{\partial\delta_{q,\mathrm{eq}}}{\partial\alpha}B_1(\rho),\\ &\tilde{C}_{32}(\rho) \coloneqq \frac{\bar{q}SdC_{Z_q}(\mathcal{M})}{mgV}; \quad \tilde{C}_{33}(\rho) \coloneqq \frac{\bar{q}SC_{Z_{\delta_q}}(\mathcal{M})}{mg}.\end{aligned}$$

The grid-based LPV model (A_G, B_G, C_G, D_G) at any flight conditions $\rho \in [\rho_j, \rho_{j+1}]$ for $j = [1,\cdots,n_g]$, results from the interpolation of the corresponding LTI realizations (A_i,B_i,C_i,D_i) of the quasi-LPV model in Eqs. (3)-(4) evaluated at the grid points, where a_i can be any interpolation method:

$$\left[\begin{array}{c|c}A_\mathrm{G}(\rho) & B_\mathrm{G}(\rho)\\ \hline C_\mathrm{G}(\rho) & D_\mathrm{G}(\rho)\end{array}\right] = \sum_{i=j}^{j+1} a_i(\rho)\left[\begin{array}{c|c}A_i & B_i\\ \hline C_i & D_i\end{array}\right]. \tag{5}$$

In particular, this approach does not require any specific model parameter dependency. However, due to the number of scheduling parameters, n_p, increasing amounts of grid points, n_g, tend to highly affect the computational cost of the synthesis process. Thus, in Section 4, an exhaustive analysis of the grid size is proposed to identify the optimal conditions for the controller design.

3. GRID-BASED CONTROLLER DESIGN

In this section, we recall the fundamental concepts related to LPV grid-based design in the robust control framework. The generalized plant architecture employed during the controller synthesis is finally presented.

3.1 Background on LPV Control Design

Most of the concepts employed here have been developed in Wu (1995). Consider the following generalized LPV plant structure:

$$\Sigma(\rho): \begin{bmatrix} \dot{x}(t) \\ z(t) \\ y(t) \end{bmatrix} = \left[\begin{array}{c|cc} A(\rho) & B_1(\rho) & B_2(\rho) \\ \hline C_1(\rho) & D_{11}(\rho) & D_{12}(\rho) \\ C_2(\rho) & D_{21}(\rho) & D_{22}(\rho) \end{array}\right] \begin{bmatrix} x(t) \\ w(t) \\ u(t) \end{bmatrix} \quad (6)$$

with states $x(t) \in \mathbb{R}^n$, control input $u(t) \in \mathbb{R}^{n_u}$, controlled outputs $z(t) \in \mathbb{R}^{n_z}$, input/output disturbances $w(t) \in \mathbb{R}^{n_w}$, measurements $y(t) \in \mathbb{R}^{n_y}$, and scheduling vector $\rho(t) \in \mathbb{R}^{n_p}$. The scheduling variables in $\rho = [\rho_1, \cdots, \rho_{n_p}]$, are supposed to be measurable in real-time, bounded in a range described by a selected set of values, and with bounded rates of variation. The investigated grid of conditions corresponds to the set of all possible combinations of the different parameter values. Additionally, the partitions $B_1(\rho) = [B_{11}(\rho),\ B_{12}(\rho)]$, $C_1(\rho) = [C_{11}(\rho),\ C_{12}(\rho)]$ hold.

In standard H_∞ gain-scheduling, local LTI controllers are individually designed at each grid point, aiming to minimize the closed-loop induced L_2-norm:

$$\|z\|_2 \leq \gamma_\infty \|w\|_2, \quad (7)$$

where the index, $\gamma_\infty > 0$, expresses the quality of the optimization results. However, no a priori guarantees are provided for controllers interpolated at generic conditions. Differently, in LPV grid-based design, a general controller $K(\rho)$ is determined through the existence of parameter-dependent Lyapunov functions, $X(\rho)$ and $Y(\rho)$ along the grid axes, that satisfy a set of Linear Matrix Inequalities (LMIs), at all the conditions described by the grid. The dependence of the Lyapunov functions from the scheduling parameters is expressed by means of scalar differentiable basis functions $\{f_i : \mathbb{R}^{n_p} \to \mathbb{R}\}_{i=1}^N$ and $\{g_i : \mathbb{R}^{n_p} \to \mathbb{R}\}_{i=1}^N$, parameterized as follows:

$$X(\rho) = X_0 + \sum_{i=1}^{N} f_i(\rho) X_i; \quad Y(\rho) = Y_0 + \sum_{i=1}^{N} g_i(\rho) Y_i \quad (8)$$

where $X_0, X_i \in \mathbb{R}^{n \times n}$ and $Y_0, Y_i \in \mathbb{R}^{n \times n}$ are unknown constant matrices derived from the resolution of the LMIs.

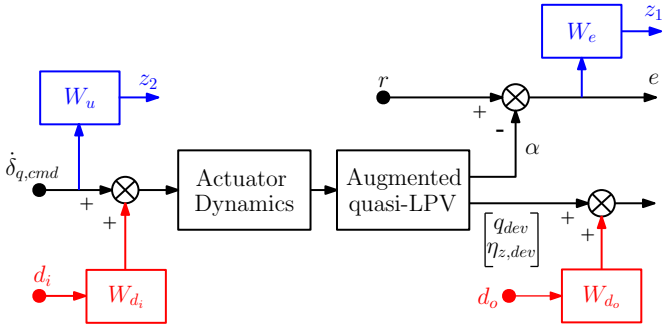

Fig. 1. Detailed control design architecture of $P(\rho)$.

Then, the generalized LPV controller structure, which satisfies the optimization constraints at each design point, is derived as in Wu et al. (1996):

$$K(\rho): \begin{bmatrix} \dot{x}_K(t) \\ u(t) \end{bmatrix} = \begin{bmatrix} A_K(\rho) & B_K(\rho) \\ C_K(\rho) & D_K(\rho) \end{bmatrix} \begin{bmatrix} x_K(t) \\ y(t) \end{bmatrix} \quad (9)$$

where:

$$\begin{aligned} A_K(\rho) = &\big[A(\rho) + \gamma_\infty^{-1}[Q^{-1}(\rho)X(\rho)L(\rho)B_{12}^T \\ &+ B_1(\rho)B_1^T(\rho)]Y^{-1}(\rho) + B_2(\rho)F(\rho) \\ &+Q^{-1}(\rho)X(\rho)L(\rho)C_2(\rho) - Q^{-1}(\rho)H(\rho,\dot{\rho})\big], \\ B_K(\rho) = &-\big[Q^{-1}(\rho)X(\rho)L(\rho)\big], \\ C_K(\rho) = &F(\rho), \end{aligned}$$

and:

$$\begin{aligned} Q(\rho) = &\big[X(\rho) - Y(\rho)^{-1}\big], \\ F(\rho) = &-\big[\gamma_\infty B_2^T(\rho)Y^{-1}(\rho) + C_{12}(\rho)\big], \\ L(\rho) = &-\big[\gamma_\infty X^{-1}C_2^T(\rho) + B_{12}(\rho)\big], \\ H(\rho,\dot{\rho}) = &-\Bigg[A_F^T(\rho)Y^{-1} + Y^{-1}A_F(\rho) + \sum_i \left(\dot{\rho}\frac{\partial Y^{-1}}{\partial \rho}\right) \\ &+\gamma_\infty^{-1}C_F^T(\rho)C_F(\rho) \\ &+\gamma_\infty^{-1}Y^{-1}(\rho)B_1(\rho)B_1^T(\rho)Y^{-1}(\rho)\big]. \end{aligned}$$

The set of LTI controllers corresponding to each point of the grid is generated as a realization of Eq. (9) at frozen ρ. A controller for any intermediate scheduling parameter values can be obtained by interpolating the previous set, as already expressed in Eq. (5). The controller synthesis is performed using the LPVTools toolbox of Matlab, introduced in Hjartarson et al. (2015).

3.2 Generalized Plant Architecture

The overall control design structure is shown in Fig. 1. Note that a second-order actuator model is included in the plant definition, G_P, and is characterized by an operating bandwidth of 150 rad/s and 0.7 damping coefficient. The main objective is to target the tracking performance of the controller by imposing a second-order weighting function, W_e, on the tracking error, $e = r - \alpha$, where r consists of a reference angle-of-attack signal generated by a *Lift-to-Drag* ratio optimization guidance law. An additional second-order filter, W_u, is applied at the actuator input to comply with the available operating bandwidth and to avoid the stall regime of the canards. Finally, constant weights, W_{d_i} and W_{d_o}, are imposed on the input and output disturbance signals, respectively, aiming to improve the controller disturbance rejection capability and to satisfy the orthogonality conditions imposed by the LPV controller synthesis, as in Wu (1995). The generalized control architecture is presented in Fig. 2, where $P(\rho)$ implements

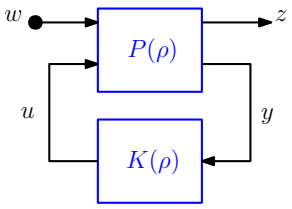

Fig. 2. Generalized LPV Plant.

the scheme of Fig. 1. The resulting generalized state vector, x_P, is augmented with the actuators and the weighting functions state variables, $x_P = [x,\, x_{\text{act}},\, x_{W_e},\, x_{W_u}]^T \in \mathbb{R}^9$. The generalized controlled output $z = [z_1,\, z_2]^T \in \mathbb{R}^2$ includes the design objectives, while tracking error, off-equilibrium pitch rate, and vertical acceleration affected by output disturbances, represent the available measurements set, $y = [e,\, (q_{\text{dev}} + W_{d_o} d_o),\, (\eta_{z,\text{dev}} + W_{d_o} d_o)]^T \in \mathbb{R}^3$. Finally, the control input, $u \in \mathbb{R}$, is the derivative of the commanded local pitch deflection, $\dot{\delta}_{q,\text{cmd}}$, while the vector of exogenous input, w, includes the reference guidance angle-of-attack trajectory, and the input/output disturbances, $w = [r,\, d_i,\, d_o]^T \in \mathbb{R}^3$. The generalized plant is evaluated at each grid point conditions, and the obtained set of LTI systems is employed for the controller synthesis.

4. GRID-BASED CONTROLLER SYNTHESIS

In this section, we discuss the complexity of the LPV control design with respect to the choice of the grid. Indeed, the amount of LMIs to be satisfied for the existence of the controller grows as a function of the number of scheduling variables, n_p, and the number of grid points, n_g, as $\mathcal{O}(n_g^{n_p})$. Additionally, even the selection of the basis functions has a relevant effect on both computational complexity and the accuracy of the optimization. For these reasons, a preliminary analysis of each scheduling variable range parameterization is proposed in the following. The analysis consists of the resolution of the controller synthesis procedure developed in LPVTools and introduced in Section 3, assuming the generalized plant in Fig. 2, and accounting for one parameter variation at a time. The parameterization is investigated as a function of:

(I) the basis functions selection, parametrized in Eq. (8);

(II) the number of considered equally spaced grid points in a common variation range;

(III) the frozen values of the other scheduling variables, selected in their ranges of variation.

The impact of (I),(II), and (III) is verified through the variation of the optimization index, γ_∞. The analysis has been extended to a wide set of basis functions and flight conditions, but only the most relevant are shown here for brevity.

4.1 Grid Analysis: Angle-of-Attack

The parameterization considers the range $\alpha \in [0,\, 12]$ deg, with bounded rates of $\dot{\alpha} \in [-10,\, 10]$ deg/s, in accordance

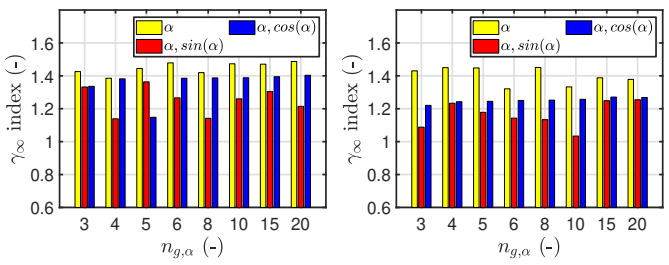

(a) (b)

Fig. 3. α gridding conditions: (a) $V = 200$ m/s, $h = 5$ km; (b) $V = 250$ m/s, $h = 9$ km.

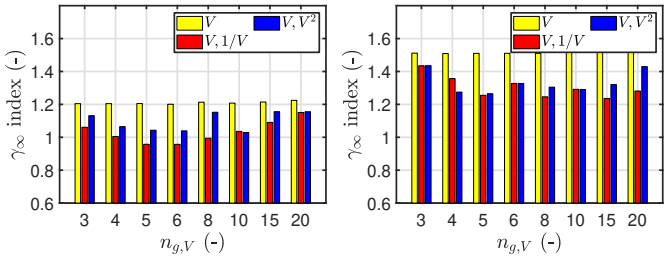

(a) (b)

Fig. 4. V gridding conditions: (a) $\alpha = 8$ deg, $h = 5$ km; (b) $\alpha = 3$ deg, $h = 13$ km.

with the expected gliding conditions. In particular, Figs. 3(a)-(b) show the synthesis results for two different $(V,\, h)$ conditions, and for a set of three different basis functions. As a general consideration, $\rho_\alpha = [\alpha,\, \sin\alpha]$ seems to provide better results both in terms of index values and impact of the n_g variation, where $f_1(\alpha), g_1(\alpha) = \alpha$ and $f_2(\alpha), g_2(\alpha) = \sin\alpha$, complying with Eq. (8). For a more accurate range representation, without exploding the final grid dimensions, $n_{g,\alpha} = 5$ points are selected.

4.2 Grid Analysis: Airspeed

The same analysis is employed for V. The results in Figs. 4(a)-(b) refer to a range of $V \in [150,\, 280]$ m/s, corresponding approximately to $\mathcal{M} \in [0.5,\, 0.9]$, and to a rate of variation of $\dot{V} \in [-5,\, 5]$ m/s^2. The system dependency on V, is more explicitly shown in Eqs. (1)-(2). Accordingly, the set of basis functions providing the best optimization with limited structural complexity is $\rho_V = [V,\, 1/V]$, with $f_1(V), g_1(V) = V$ and $f_2(V), g_2(V) = 1/V$. In reason of the quite homogeneous variation of γ_∞, a set of $n_{g,V} = 5$ points is chosen.

4.3 Grid Analysis: Altitude

Finally, the range $h \in [1,\, 13]$ km, with a bounded variation rate $\dot{h} \in [-50,\, 50]$ m/s is considered for the altitude. The results in Figs. 5(a)-(b) exhibit reliable and homogeneous optimization performances already assuming $\rho_h = [h]$ as basis functions $f_1(h), g_1(h)$. This selection will allow later reducing the overall controller synthesis complexity. Due to the wide range of altitude variation to be covered, a set of $n_{g,h} = 6$ points is preferred here.

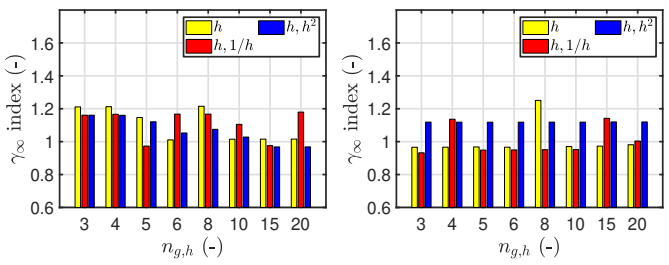

(a) (b)

Fig. 5. h gridding conditions: (a) $\alpha = 8$ deg, $V = 200$ m/s; (b) $\alpha = 13$ deg, $V = 250$ m/s.

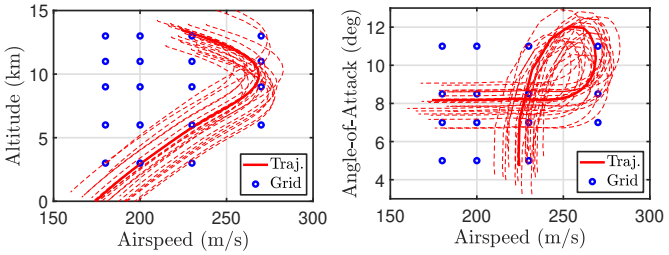

(a) (b)

Fig. 6. Scheduling variables relation: (a) guidance h/V trajectories; (b) guidance α/V trajectories.

4.4 Trajectory-based Uneven Grid Selection

The preliminary parameterization analysis results in a large set of $n_{g,\alpha} \cdot n_{g,V} \cdot n_{g,h} = 150$ grid points. However, for standard projectile applications, evenly spaced parameterizations tend to generate several grid points at inconsistent flight conditions, since the grid does not account for the relations between the scheduling variable trajectories. The employment of an uneven selection of grid points can reduce the resulting conservatism by clustering the analyzed conditions around meaningful areas of the flight envelope. Thus, a set of ad-hoc designed range-extending guidance trajectories is used for the selection of the grid values. The physical relations between the parameter trajectories are presented in Figs. 6(a)-(b), including the ideal baseline trajectories (bold red) and a set of possible variations in reason of different initial engagement conditions or selected target ranges (dashed red).

The grid size can be further minimized by investigating the stability properties of the open-loop plant in the frequency domain. The pole-zero map in Fig. 7 reveals significantly slower system dynamics at higher h and lower V values. Additionally, the stability of the system tends to increase with the amplitude of α (not shown in the figure), especially for $\alpha \geq 11$ deg. These considerations suggest the need for a denser grid at lower (α, V) conditions, and at higher h. By combining stability and parameter relations information, it is possible to reduce the number of grid points to $n_g = 80$, as shown in Figs. 6(a)-(b), by selecting:

- $\alpha = [5\ 7\ 8.5\ 11]$ deg;
- $V = [180\ 200\ 230\ 270]$ m/s;
- $h = [3\ 6\ 9\ 11\ 13]$ km.

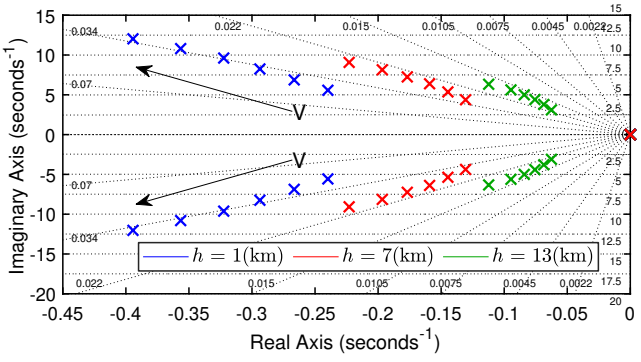

Fig. 7. Pole-Zero map variation at different (V, h) conditions, and for a stable $\alpha = 12$ deg.

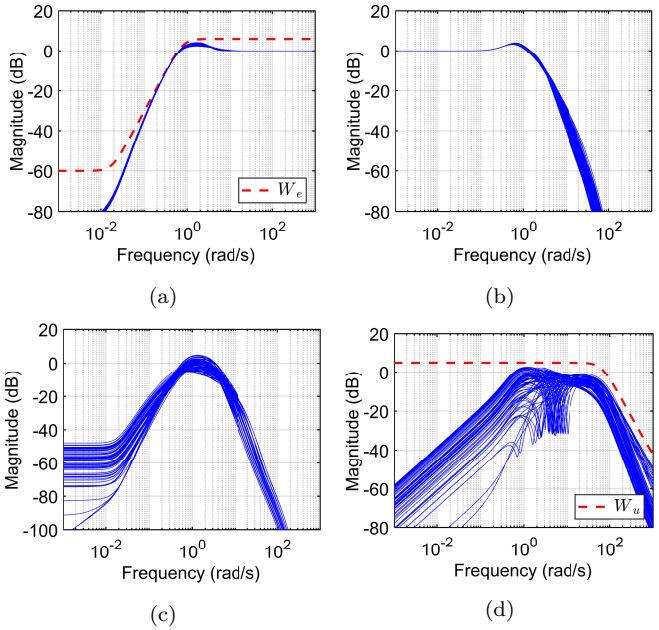

(a) (b) (c) (d)

Fig. 8. Frequency results: (a) Sensitivity functions (S_o); (b) Complementary Sensitivity (T_o); (c) Plant Sensitivity (S_oG); (d) Controller Sensitivity (KS_o).

By reducing the number of grid points the amount of LMIs to be satisfied in the controller synthesis decreases approximately to $\mathcal{O}(80^3)$. Moreover, the dependence of the obtained controllers on the parameters' variation rates, expressed in Eq. 9, is relaxed to minimize the implementation complexity. Thus, the number of controllers being implemented and interpolated in simulation reduces to 80.

5. LPV GRID-BASED CONTROLLER ANALYSIS

The overall LPV controller synthesis is based on the 3D grid described by the 80 uneven points selection discussed in Section 4. The design architecture and optimization objectives were presented in Section 3. The performances of the controller are first verified in the frequency domain. Finally, a trajectory tracking simulation is proposed, assuming a gliding phase flight scenario.

5.1 Frequency Domain Analysis

The frequency domain performances resulting from the controller synthesis are shown in Figs. 8. The Sensitivity functions (S_o) in Fig. 8(a) present a resonance, which increases at more unstable flight conditions. Additionally, the controller bandwidth is limited by the responsiveness of the system, affecting the tracking capability. However, these results are consistent with the characteristics of the projectile in terms of reduced control authority and maneuverability. Indeed, the expected gliding trajectories are supposed to impose smooth variations of the scheduling parameters, as well as a reduced effort of the front control canards. The optimization index value, $\gamma_\infty = 1.14$, confirms that the controller specifications are almost perfectly met. The controller is characterized by reasonable high-frequency noise attenuation properties, as expressed by the Complementary Sensitivity (T_o) curves in Fig. 8(b), and low-frequency disturbance rejection properties, shown by

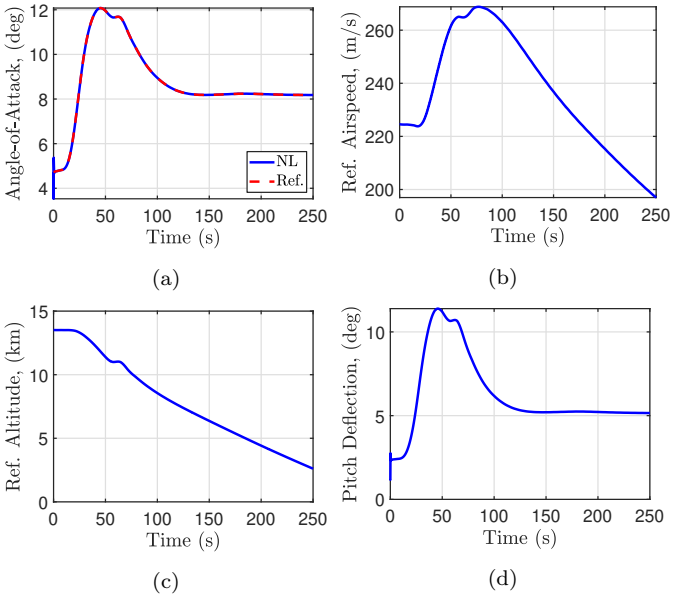

Fig. 9. Simulation trajectories: (a) angle-of-attack; (b) ref. airspeed; (c) ref. altitude; (d) pitch deflection.

the Plant Sensitivity (S_oG) functions in Fig. 8(c). Finally, Fig. 8(d) exhibits the boundaries imposed on the control effort, where the bandwidth is limited to the available one characterizing the actuator dynamics. The Controller Sensitivity (KS_o) peak values belong to the curves corresponding to highly unstable fight conditions, where more authority is required to ensure stability and performance.

5.2 Time Domain Trajectory Tracking Simulation

The LPV controller is finally tested on the original nonlinear model of the projectile pitch channel dynamics, through a trajectory tracking simulation scenario. The reference angle-of-attack signal is the result of an ad-hoc *Lift-to-Drag* guidance optimization, designed to maximize the range performance of the projectile. Since the dynamics of the exogenous scheduling variables (V and h) are not described by the model in Eqs. (1)-(2), the corresponding set of guidance trajectories is coherently employed. These curves have been obtained using a planar point-mass model of the projectile. The simulation addresses a gliding phase scenario, where the engagement of the guidance signals occurs at the apogee of the projectile ballistic trajectory, after the deployment of the canards.

The initial oscillation in Fig. 9(a), derives from the sudden variation of α due to the additional canards' lift contribution after the deployment instant. Indeed, during the initial ballistic phase, α tends to remain very low keeping the projectile aligned with the trajectory. However, the oscillation is rapidly compensated by the controller. An important remark concerns the total deflection angle perceived by the canards, α_{can}. It is defined as the linear superposition between the local pitch deflection imposed by the controller (δ_q), and the overall α trajectory performed by the projectile body, as $\alpha_{\text{can}} = \alpha + \delta_q$. The maximum effort imposed on the canards in Fig. 9(d) is far below their characteristic limit of saturation ($\alpha_{\text{can}} < 25$ deg), thus avoiding any risk of stall conditions. During the simulation, the trajectories of scheduling variables (α, V, h) reach across most of the flight envelope described by the grid, as a confirmation of the controller performances and the advantages of the uneven parameterization.

6. CONCLUSION

In this paper, an LPV grid-based model representing the pitch channel dynamics of a guided projectile is investigated. The model is employed for the synthesis of a pure LPV/H_∞ loop-shaping autopilot design. As a crucial aspect of the grid-based approach, the selection of the grid size is extensively investigated for a set of three scheduling parameters (α, V, h). A trajectory-based uneven grid points selection is proposed to minimize the conservatism generated by the inclusion of inconsistent flight conditions in the controller synthesis. The performances are assessed both in the frequency domain and through a guidance-based trajectory tracking simulation.

REFERENCES

Biannic, J.M. and Apkarian, P. (1999). Missile autopilot design via a modified LPV synthesis technique. *Aerospace Science and Technology*, 3(3), 153–160.

Bryson, J. and Gruenwald, B.C. (2022). Linear parameter varying model predictive control of a high-speed projectile. In *AIAA Scitech 2022 Forum*, 1585.

Gruenwald, B.C. and Bryson, J. (2022). A gain-scheduled approach for the control of a high-speed guided projectile. In *AIAA Scitech 2022 Forum*, 0612.

Hjartarson, A., Seiler, P., and Packard, A. (2015). LPVTools: A toolbox for modeling, analysis, and synthesis of parameter varying control systems. *IFAC-PapersOnLine*, 48(26), 139–145.

Sato, M. (2022). From impractical LPV controllers to practical and "implementable" LPV controllers: Verification with research airplane. In *5th IFAC Workshop on Linear Parameter Varying Systems (LPVS)*. Montreal, Canada. Plenary talk.

Shamma, J.S. (1988). Analysis and design of gain scheduled control systems. Ph.D. dissertation.

Shamma, J.S. and Athans, M. (1992). Gain scheduling: Potential hazards and possible remedies. *IEEE Control Systems Magazine*, 12(3), 101–107.

Theodoulis, S., Sève, F., and Wernert, P. (2015). Robust gain-scheduled autopilot design for spin-stabilized projectiles with a course-correction fuze. *Aerospace Science and Technology*, 42, 477–489.

Vinco, G.M., Theodoulis, S., and Sename, O. (2022a). Flight dynamics modeling and simulator design for a new class of long-range guided projectiles. In *CEAS EuroGNC Conference*. Berlin, Germany.

Vinco, G.M., Theodoulis, S., Sename, O., and Strub, G. (2022b). Quasi-LPV modeling of guided projectile pitch dynamics through state transformation technique. In *5th IFAC Workshop on Linear Parameter Varying Systems (LPVS)*. Montreal, Canada.

Wu, F. (1995). *Control of linear parameter varying systems*. University of California, Berkeley. Ph.D. dissertation.

Wu, F., Yang, X.H., Packard, A., and Becker, G. (1996). Induced L2-norm control for LPV systems with bounded parameter variation rates. *International Journal of Robust and Nonlinear Control*, 6(9-10), 983–998.